J. Fluid Mech. (1991), *vol.* 226, *pp.* 63–89
Printed in Great Britain

Oscillations of liquid captive rotating drops

By A. M. GAÑÁN-CALVO
Escuela Técnica Superior de Ingenieros Industriales, Universidad de Sevilla, 41012 Sevilla, Spain

(Received 8 March 1990 and in revised form 6 October 1990)

A linear analysis of the free oscillations of captive drops or bubbles is discussed. The drop is surrounded by an immiscible liquid or gas and undergoes rotation as a rigid body in the presence of gravity. Using spectral analytical methods, we provide a general formulation for both elliptic and hyperbolic oscillation regimes of the frequency spectrum, for any combination of the Weber and Bond numbers. The method uses a Green function to reduce the inviscid Navier–Stokes equations and boundary conditions to an eigenvalue problem. Both the Green function and normal velocities at the interface are expanded in the orthogonal functional space generated by the Sturm–Liouville problem associated to the interface equation. The effect on the vibration modes of the density and geometrical parameters of the captive drop and surrounding medium is analysed. We present a complete analysis of the low-frequency spectra in the elliptic regime of a set of floating liquid zones and captive drops for a continuous range of Weber and Bond numbers. It is shown that, depending on the geometrical parameters of the system, the elliptic vibration spectrum presents a *sui generis* modal interaction for low wavenumbers and certain ranges of Weber number.

1. Introduction

Since the pioneering contributions of Laplace, Young and Poisson to the mathematical formulation of the equilibrium configurations of liquid menisci and the early experimental work of Plateau, capillary fluid mechanics has undergone an intense study and development.

Owing to the simplicity of the governing equations, the stability limits and free vibrations for simple geometries (spherical, cylindrical, or flat equilibrium shapes) were the first issues under study. An excellent and thorough review of the literature on this field can be found in Myshkis *et al.* (1987). These early studies involved a linearization of both the equation of the free surface given by the balance of dynamical pressures, and the equations of motion of the fluids. Thus, after the appropriate choice of coordinates, the equation of the perturbation of the interface, which in turn determines the complexity of the problem, can be analytically solved. However, although many mechanical features of capillary menisci came to light, the assumptions made in dealing with these simple geometries were quite restrictive.

For many axisymmetric equilibrium configurations, the effect of the presence of mass forces such as gravitational (Pitts 1974, 1976), isorotational (Brown & Scriven 1980*a*, *b*) or electromagnetic fields (Basaran & Scriven 1989; González *et al.* 1989) as well as thermal effects (Busse 1984; Chifu *et al.* 1983) have also been investigated in the linear stability regime for both single and compound drops, either isolated or captive. However, the presence of these body forces was investigated only in the cases when they could be treated as small perturbations, or in such a way that they

do not affect the simplicity of the equilibrium shape. Therefore, they appear as an additional term in the equation of the interface perturbation.

Hence, the solution of a more general approach to the linear dynamics of captive liquid menisci is still under discussion. Several studies have been recently presented for simple geometries (spherical, Strani & Sabetta 1984, 1988; and cylindrical, Sanz 1985; Sanz & López Díez 1989) in the absence of mass forces such as rotation or gravity. The application of numerical techniques to integrate the general boundary problem for non-trivial shapes provides an essential tool for the comprehension and quantification of the effects of several mass forces.

In this paper, we analyse the inviscid free vibrations of axisymmetric floating liquid zones (liquid bridges) and pendent or sessile drops or bubbles surrounded by an immiscible incompressible fluid under the combined influence of both gravitational and isorotational (the drop and its surroundings are assumed to be rotating as a rigid body) fields.

The analytical method to be used is based on the Sturm–Liouville structure of the second-order linear differential equation which governs the normal small disturbances of the interface (Gañán & Barrero 1986). This differential equation is defined in a curvilinear coordinate system (Boucher & Evans 1975) along a meridian of the axisymmetric equilibrium profile. The homogeneous part of this equation is written as a second-order differential operator which defines a Hilbert functional space. The corresponding integral operator is defined using Green's theorem (Butkov 1968) and the Hilbert space. Therefore, the normal perturbation of the interface can be explicitly written. Equating the normal perturbation to the normal velocities on the interface and making use of the equation for the normal disturbances and the linearized Navier–Stokes equations for the inviscid motion, one obtains an explicit expression for the dynamical pressures on the interface and its derivatives. Finally, the problem is formulated as a classical Neumann-type boundary problem for the dynamic pressure, which can be solved by several techniques (spectral methods, Green function methods, finite differences, etc.).

Regardless of the complexity of the equilibrium shape, the method introduced by Gañán & Barrero (1986) possesses great generality since it yields the solution of the free oscillations of the meniscus under study for arbitrary combinations of the Bond and Weber numbers (B and W respectively). Using a similar approach, Myshkis *et al.* (1987) obtained some numerical results for menisci formed by an isorotating liquid partially filling a cylindrical vessel in the absence of gravity. Myshkis' results have shown many of the essential features of the oscillation frequency spectra of isorotating liquid axisymmetric menisci. In particular, their results showed the splitting of the spectrum into two sets, one corresponding to an elliptical regime and the other to a hyperbolic one. However, a deeper study on the gyroscopic effects on the elliptical frequency spectrum of rotating liquid menisci under the influence of a gravitational field still remains to be done. Here, using separation of variables (a well-known form of the Ritz method), we report some general results for rotating captive drops in the absence of gravity as well as an analysis of the elliptic spectrum of two typical rotating liquid bridges under the influence of gravity. We have chosen this method for two reasons: (*a*) it is capable of dealing with most of the stable equilibrium shapes, allowing us to analyse the basic effects of the boundary conditions, geometries of support and vessel, etc. and (*b*) for a given accuracy, it is one or two orders of magnitude faster than other numerical schemes. The limits of convergence of this method are sharp and can be marked out as a function of the Bond and Weber numbers. This study will be given elsewhere. Here we present some

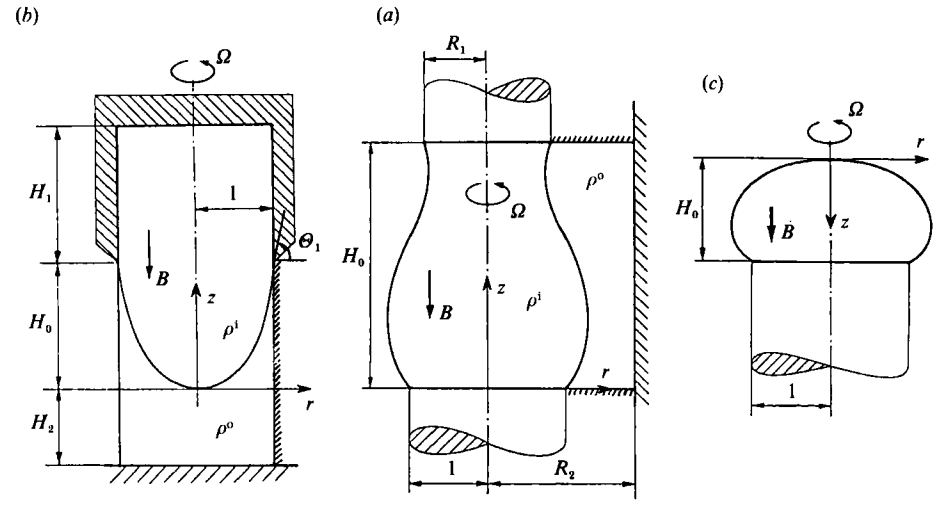

FIGURE 1. (*a*) Liquid bridge, (*b*) pendant and (*c*) sessile drop configurations.

new effects of the gyroscopic forces and a somewhat general description of how the rotation affects the frequency spectrum, depending on the boundary conditions and the difference of the densities of the inner and outer fluids.

However, there are limitations in the use of the separation of variables for the case of some extreme captive drops configurations (i.e. slender, pendant drops or very flat, overflowing, sessile drops), due to the lack of convergence of the method for these configurations. Consequently, a numerical scheme more independent of the geometrical constraints such as those based on the Green methods (e.g. boundary-elements method) has to be applied. Some results using a boundary-element method are presented in Gañán & Barrero (1990), and more general results applying this method will be presented elsewhere.

In §2 we write the equations and boundary conditions of the linear problem under consideration. A detailed description of the method of solving the dynamical problem is given in §3, and the derivation of a dispersion relation is discussed in §4, where the method of separation of variables is applied. Numerical results on the limits of convergence are presented in §5, and a discussion of the results is given in §6.

2. Formulation of the problem

Let us consider the small-amplitude free vibrations of a liquid captive drop or bubble which forms an axisymmetric system together with its surrounding medium and cylindrical container (figure 1). The liquid or gas volume V may be held between two parallel, coaxial disks (liquid bridge configuration), or be in contact with a single coaxial support (pendant or sessile drop configurations). The non-dimensional Navier–Stokes equations for the inviscid motion of both inner and outer incompressible fluids read

$$\nabla \cdot \boldsymbol{v}^j = 0, \tag{1}$$

$$\frac{\mathrm{D}\boldsymbol{v}^j}{\mathrm{D}t} = -\nabla\left(\frac{p^j}{\rho^j} + \frac{B}{\rho^i - \rho^o} z + \frac{W}{\rho^i - \rho^o}\frac{(\boldsymbol{k} \wedge \boldsymbol{x})^2}{2}\right) - 2\left(\frac{W}{\rho^i - \rho^o}\right)^{\frac{1}{2}} \boldsymbol{k} \wedge \boldsymbol{v}^j, \tag{2}$$

where superscript j = o, i refers to outer or inner fluid respectively. The whole system is assumed to be rotating as a rigid body, and the drop dynamics is then described

in a coordinate system solidly rotating with both inner and outer fluids. In what follows we will use cylindrical coordinates $\boldsymbol{x}(r,\varphi,z)$. The acceleration due to gravity $\boldsymbol{g}$ and the rotation constant speed $\tilde{\boldsymbol{\Omega}}\boldsymbol{k}$ are taken along the z-axis. Only positive rotation speeds are considered since, owing to the symmetry, no additional results can arise for negative rotation. All variables in (1), (2) and figure 1 have been non-dimensionalized using a reference density $\tilde{\rho} = \tilde{\rho}^{\mathrm{i}} + \tilde{\rho}^{\mathrm{o}}$, a characteristic length $\tilde{R}_0$ which is either the bottom radius for bridges or the support radius for drops, and a characteristic time $t_{\mathrm{c}} = (\tilde{\rho}\tilde{R}_0^3\sigma^{-1})^{\frac{1}{2}}$, where σ and $\tilde{\rho}^j$ are surface tension and dimensional density respectively. The Bond and Weber numbers are defined as $B \equiv g(\tilde{\rho}^{\mathrm{i}} - \tilde{\rho}^{\mathrm{o}})\tilde{R}_0^2\sigma^{-1}$ and $W \equiv \tilde{\Omega}^2(\tilde{\rho}^{\mathrm{i}} - \tilde{\rho}^{\mathrm{o}})\tilde{R}_0^3\sigma^{-1}$ respectively.

We assume that the ratio between viscous and inertial forces is very small:

$$\frac{1}{t_{\mathrm{c}}} \gg \frac{\nu}{\tilde{R}_0^2},$$

so that

$$(\nu^{j^2}\tilde{\rho}\sigma^{-1}\tilde{R}_0^{-1})^{\frac{1}{2}} \ll 1.$$

In this limit, a small amount of the oscillation energy is dissipated in thin boundary layers of thickness

$$\delta \sim (\nu^2\tilde{\rho}\tilde{R}_0^3\sigma^{-1})^{\frac{1}{4}} \ll \tilde{R}_0,$$

existing at solid surfaces and fluid interfaces. Consequently, a second-order damping effect is expected to take place when oscillation goes on for a long time compared with the inverse of the frequency. Our analysis represents the first-order approximation to the dynamics of captive drops of liquids of very low viscosity (e.g. water, water-based solutions, most melted metals and minerals, many organic liquids, blood, etc.). Studies of the errors for the inviscid limit can be found, for spherical free drops, in Miller & Scriven (1968), and for spherical captive drops, in Strani & Sabetta (1988).

Equations (1) and (2) must be solved subject to the following boundary conditions:

(i) The normal component of the velocity must be continuous across the interface and vanish on the solid surfaces.

(ii) The interfacial surface behaves as a fluid surface, i.e. if the interface is described using a function $f(r,\varphi,z,t) \equiv F(\varphi,z,t) - r$ being equal to zero at the surface, it must satisfy the equation

$$\frac{\mathrm{D}f}{\mathrm{D}t} = \frac{\partial f}{\partial t} + \boldsymbol{v}^j \cdot \boldsymbol{\nabla} f = 0. \tag{3}$$

(iii) The pressure jump across the interface is balanced only by surface tension:

$$p^{\mathrm{i}} - p^{\mathrm{o}} = \boldsymbol{\nabla} \cdot \boldsymbol{n}, \tag{4}$$

$\boldsymbol{n}$ being the outward unit normal on the interface.

(iv) The liquid volume V of the bridge or captive drop is kept constant.

System (1)–(2) and conditions (i)–(iv) form a boundary problem whose solution determines the interface position as a function of the space coordinates and time.

To analyse the small free oscillations of the system we use the classical normal mode decomposition and, consequently, expand the solution as a small perturbation from the equilibrium (Lamb 1932; Rayleigh 1945; Greenspan 1968; Myshkis *et al.* 1987, etc.):

$$F(\varphi,z,t) = F_{\mathrm{e}}(z) + \sum_{m=-\infty}^{\infty}\sum_{n=1}^{\infty} \eta_{m,n}(z)\exp\left[\mathrm{i}(m\varphi - \omega_{m,n}t)\right], \tag{5}$$

$$p^j(r,\varphi,z,t) = p^j_{\mathrm{e}}(r,z) + \sum_{m=-\infty}^{\infty}\sum_{n=1}^{\infty} \rho^j \Phi^j_{m,n}(r,z)\exp\left[\mathrm{i}(m\varphi - \omega_{m,n}t)\right], \tag{6}$$

$$\boldsymbol{v}^j = 0 + \sum_{m=-\infty}^{\infty} \sum_{n=1}^{\infty} \begin{Bmatrix} u^j_{m,n}(r,z) \\ v^j_{m,n}(r,z) \\ w^j_{m,n}(r,z) \end{Bmatrix} \exp\left[\mathrm{i}(m\varphi - \omega_{m,n}\, t)\right], \tag{7}$$

where F is the non-dimensional interface radius and subscript e refers to the axisymmetric equilibrium conditions. The perturbations quantities $|\eta_{m,n}|$ and $|\rho^j \Phi^j_{m,n}|$ are much smaller than F_e and p^j_e, respectively; m stands for the aximuthal wavenumber and $\omega_{m,n}$ is the nth natural frequency of the system for a given m. If $W \neq 0$, it is worth mentioning that for a given m and n, $\omega_{m,n} \neq \omega_{,m,n}$ (Myshkis *et al.* 1987). Only the axisymmetric mode ($m = 0$) consists of an azimuthal standing wave. Nevertheless, when $W = 0$, it can be proved that $\omega_{m,n} = \omega_{-m,n}$ and one may add together a backward and a forward mode of the sample amplitude to obtain an azimuthal standing wave, giving rise, seemingly, to a 'transverse' mode.

Taking into account expansions (5)–(7), the first-order terms of system (1)–(2) and conditions (i)–(iv) constitute the well-known equilibrium problem that determines the captive drop equilibrium shape (Padday 1971; Boucher & Evans 1975, among many others). In what follows, subscripts r and z stand for $\partial/\partial r$ and $\partial/\partial z$ respectively. Furthermore, for simplicity, subscripts m, n are dropped in the notation.

The second-order problem gives the radial disturbance of the interface η:

$$\frac{1}{F_e}\left\{\left[\frac{F_e \eta_z}{(1+F^2_{e_z})^{\frac{3}{2}}}\right]_z + \left[\frac{(1-m^2)}{F_e(1+F^2_{e_z})^{\frac{1}{2}}} + WF^2_e\right]\eta\right\} + [\rho^i \Phi^i - \rho^o \Phi^o]_{r=F_e(z)} = 0, \tag{8}$$

together with the disturbances in the pressure and velocity fields of both fluids (Greenspan 1968):

$$\frac{1}{r}(r\Phi^j_r)_r + (1-\lambda^2)\,\Phi^j_{zz} - \frac{m^2}{r^2}\Phi^j = 0, \tag{9}$$

$$\left.\begin{aligned} \mathrm{i}\omega u^j &= \Phi^j_r - 2\Omega v^j \\ \mathrm{i}\omega v^j &= \frac{\mathrm{i}m\Phi^j}{r + 2\Omega u^j} \\ \mathrm{i}\omega w^j &= \Phi^j_z \end{aligned}\right\} \Rightarrow \left.\begin{aligned} \mathrm{i}\omega u^j &= \frac{\Phi^j_r - \lambda m \Phi^j / r}{1-\lambda^2} \\ \mathrm{i}\omega v^j &= -\frac{\mathrm{i}(\lambda \Phi^j_r - m\Phi^j/r)}{1-\lambda^2} \\ \mathrm{i}\omega w^j &= \Phi^j_z \end{aligned}\right\}, \tag{10}$$

where

$$\Omega = \left(\frac{W}{\rho^i - \rho^o}\right)^{\frac{1}{2}}$$

and

$$\lambda = \frac{2\Omega}{\omega}.$$

Equations (8) and (9) and relations (10) must be solved subject to the conditions

$$\eta(0) = 0, \quad \eta(H_0) = 0, \tag{11}$$

$$u^j = 0 \quad \text{on solid surfaces } r = \text{const.},$$

and

$$w^j = 0 \quad \text{on solid surfaces } z = \text{const.}$$

The requirement of continuity of the normal velocity across the interface yields

$$\mathrm{i}\omega\eta = [-u^j + w^j F_{e_z}]_{r=F_e(z)}. \tag{12}$$

Finally, the constant-volume condition reads

$$\int_0^{2\pi} \int_0^{H_0} \eta F_e \exp(\mathrm{i}m\varphi)\, \mathrm{d}z\, \mathrm{d}\varphi = 0. \tag{13}$$

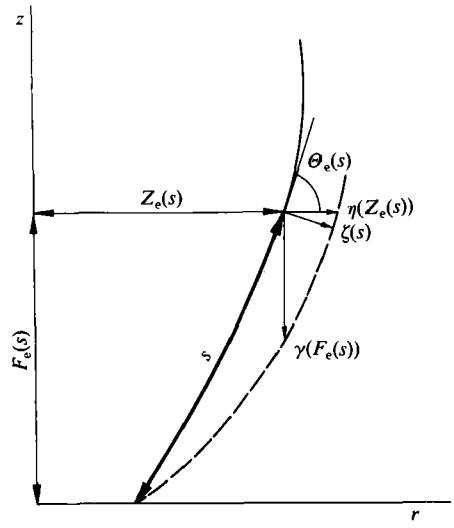

FIGURE 2. Intrinsic coordinate s along the equilibrium shape. The sketch shows the radial $\eta(z)$, normal $\zeta(s)$, and vertical $\gamma(r)$ disturbances.

Note that if $m \neq 0$, (13) is satisfied for any value of η, and if $m = 0$ reduces to

$$\int_0^{H_0} \eta F_e \, dz = 0. \tag{14}$$

System (8)–(10) with conditions (11)–(13) defines a homogeneous eigenvalue problem for a given equilibrium shape $F_e(z)$. Its solution determines the natural frequency spectrum for each azimuthal wavenumber m.

3. Solution of the problem

Introducing an intrinsic coordinate along the undisturbed equilibrium shape F_e, and writing the normal disturbance $\zeta(s)$ as (Gañán & Barrero 1986)

$$\zeta(s) = \eta[Z_e(s)] \sin\Theta_e(s), \tag{15}$$

where $Z_e(s)$ and $\Theta_e(s)$ are the vertical coordinate and the slope angle of the equilibrium shape, respectively (figure 2), equation (8) is now written in terms of $\zeta(s)$ as follows (see Appendix A):

$$\frac{1}{F_e}\frac{d}{ds}\left(F_e \frac{d\zeta}{ds}\right) + q(s,m)\,\zeta = (\rho^o \Phi^o - \rho^i \Phi^i)_{r=F_e(s)}, \tag{16}$$

where

$$q(s,m) = B\cos\Theta_e + \left(\frac{d\Theta_e}{ds}\right)2 + \frac{\sin^2\Theta_e}{F_e^2} + WF_e \sin\Theta_e - \frac{m^2}{F_e^2}. \tag{17}$$

We assume

(*a*) The contact line of the meniscus with the solid surfaces is to be fixed:

$$\zeta(0) = 0, \quad \zeta(s_0) = 0 \quad \text{(bridges)}, \tag{18}$$

$$\left.\begin{aligned} \zeta(0) &= 0 \quad \text{if } m \neq 0 \\ \left.\frac{d\zeta}{ds}\right|_{s=0} &= 0 \quad \text{if } m = 0 \end{aligned}\right\} \zeta(s_0) = 0 \quad \text{(drops)}, \tag{19}$$

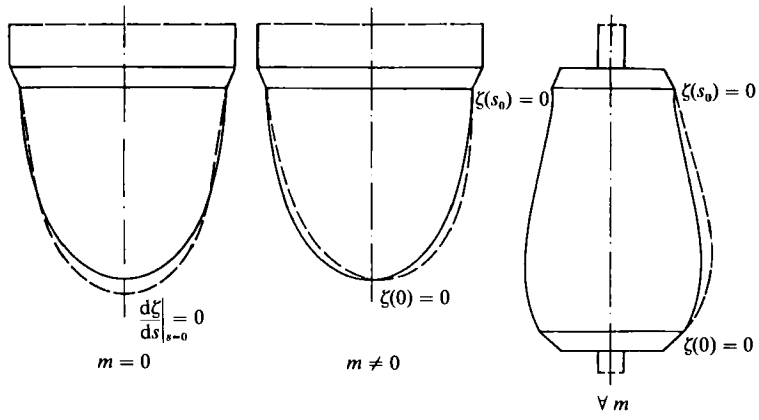

FIGURE 3. Boundary conditions for bridge and drop deformations. Notice the difference in the boundary conditions for symmetric and non-symmetric drop deformation.

where s_0 is the total length of the equilibrium interface profile. Notice that the drop condition at $s = 0$ does not arise from the anchorage (like in the case of liquid bridges), but from the nature of the interface motion, symmetric ($m = 0$) or non-symmetric ($m \neq 0$), (figure 3). (Other anchoring conditions could be defined. In §5.2 we present, for comparison with existing results (Myshkis *et al.* 1987), the case of a liquid drop inside a tube with slipping contact line.)

(*b*) The continuity of normal velocities across the interface, (12), is now written as

$$i\omega\zeta = \left[-\frac{dZ_e}{ds}u^j + \frac{dF_e}{ds}w^j\right]_{r=F_e(s)} \tag{20}$$

where $i\omega\zeta$ is the Eulerian interface velocity.

(*c*) The constant-volume condition for ($m = 0$), (15), reduces to

$$\int_0^{s_0} \zeta(s)\, F_e(s)\, ds = 0. \tag{21}$$

From the Sturm–Liouville character of (16) with (18)–(20), an orthogonal functional space

$$\{\zeta_q^*(s)\}_{q=1,2,\ldots,\infty},$$

can be defined in the interval $(0, s_0)$. These eigenfunctions are solutions satisfying the following Sturm–Liouville problem for any of the eigenvalues l_q:

$$\frac{1}{F_e}\frac{d}{ds}\left(F_e\frac{d\zeta_q^*(s)}{ds}\right) + [q(s,m) - l_q]\,\zeta_q^*(s) = 0, \tag{22}$$

with conditions (18)–(19).

The eigenfunctions ζ_q^* satisfy orthogonality conditions since they are solutions of a Sturm–Liouville problem:

$$\int_0^{s_0} F_e(s)\,\zeta_q'(s)\,\zeta_k'(s)\,ds = \begin{cases} 0, & k \neq q \\ D_q > 0, & k = q \end{cases}. \tag{23}$$

Equation (16) may be expressed as a differential operator applied on the normal disturbance $\zeta(s)$:

$$\Psi(\zeta(s)) \equiv \frac{1}{F_e}\frac{d}{ds}\left(F_e\frac{d\zeta_q^*(s)}{ds}\right) + q(s,m)\,\zeta(s) = \rho^o\,\Phi^o(s) - \rho^i\,\Phi^i(s). \tag{24}$$

Now, the Green-function method can be used for this problem to calculate the inverse integral operator Ψ^{-1} which formally yields

$$\zeta = \Psi^{-1}(\rho^{\mathrm{o}}\,\Phi^{\mathrm{o}} - \rho^{\mathrm{i}}\,\Phi^{\mathrm{i}}). \tag{25}$$

This operator can be expressed in terms of the functional space $\{\zeta_q^*\}$ as (Appendix B):

$$\Psi^{-1}(\tau(\xi)) = \sum_{q=1}^{\infty} \frac{\int_0^{s_0} (\tau(\xi))\,\zeta_q^*(\xi)\,F_{\mathrm{e}}(\xi)\,\mathrm{d}\xi}{l_q\,s\int_0^{s_0} \zeta_q^{*2}(\xi)\,F_{\mathrm{e}}(\xi)\,\mathrm{d}\xi}\,\zeta_q^*(s). \tag{26}$$

Taking into account (10), kinematic condition (20) may be written as

$$\omega^2(1-\lambda^2)\sum_{q=1}^{\infty} \frac{\int_0^{s_0} (\rho^{\mathrm{o}}\,\Phi^{\mathrm{o}}(\xi) - \rho^{\mathrm{i}}\,\Phi^{\mathrm{i}}(\xi))\,\zeta_q^*(\xi)\,F_{\mathrm{e}}(\xi)\,\mathrm{d}\xi}{l_q\int_0^{s_0} \zeta_q^{*2}(\xi)\,F_{\mathrm{e}}(\xi)\,\mathrm{d}\xi}\,\zeta_q^*(s)$$

$$= \sin\Theta_{\mathrm{e}}[\Phi_r^j - \lambda m\Phi^j/r]_{r=F_{\mathrm{e}}} - (1-\lambda^2)\cos\Theta_{\mathrm{e}}[\Phi_z^j]_{z=Z_{\mathrm{e}}},\quad j = \mathrm{i},\,\mathrm{o}. \tag{27}$$

Finally, multiplying both sides of (27) by

$$\zeta(s)\,F_{\mathrm{e}}(s)\,\mathrm{d}s$$

and integrating them between 0 and s_0, one may write the homogeneous boundary problem of the Neumann type for the state function Φ^j (Greenspan 1968; Myshkis *et al.* 1987):

$$\nabla^2\Phi^j = \lambda^2\frac{\partial^2\Phi^j}{\partial z^2} \tag{28}$$

with boundary conditions given by

(i) at the interface:

$$\frac{\omega^2(1-\lambda^2)}{l_q}\int_0^{s_0} (\rho^{\mathrm{o}}\,\Phi^{\mathrm{o}}(\xi) - \rho^{\mathrm{i}}\,\Phi^{\mathrm{i}}(\xi))\,\zeta_q^*(\xi)\,F_{\mathrm{e}}(\xi)\,\mathrm{d}\xi$$

$$= \int_0^{s_0} \{\sin\Theta_{\mathrm{e}}[\Phi_r^j - \lambda m\Phi^j/r]_{r=F_{\mathrm{e}}(\xi)} - (1-\lambda^2)\cos\Theta_{\mathrm{e}}[\Phi_z^j]_{z=Z_{\mathrm{e}}(\xi)}\}\,\zeta_q^*(\xi)\,F_{\mathrm{e}}(\xi)\,\mathrm{d}\xi,$$

$$q = 1, \ldots, \infty,\quad j = \mathrm{i},\,\mathrm{o} \tag{29}$$

(ii) at the solid boundaries:

$$n_r^j\,\Phi_r^j + n_z^j\,\Phi_z^j = 0, \tag{30}$$

n_z^j and n_r^j being the components of the outer normal unit vector to the solid boundaries of medium j. When $m = 0$, the constant-volume condition (21) allows a particular solution of (28) $\Phi^j = \text{const.}$, to be calculated.

Depending on the value of λ in (28), the problem has elliptic ($\lambda^2 < 1$) or hyperbolic ($\lambda^2 > 1$) character (Myshkis *et al.* 1987). Therefore, since $\lambda^2 = 4\Omega^2/\omega^2$, the frequency spectrum is split into two sets: one ($\omega^2 \in (4\Omega^2, \infty)$) corresponds to oscillation modes whose motions consist of surface waves, and the other $\{\omega^2 \in (0, 4\Omega^2)\}$, characteristic for a rotating liquid, is due to internal waves occurring over the entire volume (Greenspan 1968). As general remark, it should be pointed out that the hyperbolic spectrum is dense on the interval $(0, 2\pi)$, while the elliptic one is countable on $(2\pi, \infty)$ and $\omega_{m,n} \to \infty$ as $m \to \infty$ or $n \to \infty$.

The final unknowns of (28) with conditions (30) and (29) are the state function Φ^j and the eigenvalue $\lambda = 2\Omega/\omega$. Nevertheless, Φ^j must be solved at the interface using

a functional basis different from $\{\zeta_q^*\}$ since, in general, neither the equilibrium interface fits with any coordinate surface (in this case plane or cylindrical surfaces) nor are $\{\zeta_q^*\}$ solutions of (28) at the interface. Several methods, each of them using a different functional basis to represent the unique solution Φ^j of a particular problem, can be applied to find approximate solutions for equation (28):

(*a*) Expanding Φ^j in a sequence of linearly independent functions $\Phi_k^*(r, z)$ which are solutions to (28) with condition (30). In cylindrical coordinates, the most appropriate bases are the cylindrical harmonics, Bessel and circular functions (Ritz method). Thereafter, a subsequent numerical approach to Φ^j by its expansion on the discrete set of functions $\{\Phi_k^*(r, z)\}_{k=1,\ldots,N}$ must be carried out.

(*b*) Using an integral formulation of the boundary problem such as Green's method (which gives rise to the boundary-elements method, or the panel method in aerodynamics) or a weighted residual method. The choice of the basis is now closely related to the boundary discretization: usually, the basis consists of smooth polynomial splines which vanish over all the elements except on the one under consideration. However, those methods only apply to elliptic problems.

(*c*) In the case of the hyperbolic regime, the method of characteristics may be an alternative to the Ritz method. The boundaries must also be discretized as in (*b*). Nevertheless, a great disadvantage of the method of characteristics is that the characteristics surfaces are not known *a priori*: they are cones whose semi-angle is a function of the eigenvalues $\lambda = 2\Omega/\omega$ (Greenspan 1968).

The boundary elements method – although the most appropriate in the case of a vessel of complex geometry – requires about 50 times the computing time needed to solve the same case by the separation of variables. However, this latter method proves able to yield sufficiently accurate results for the influence of the physical and main geometrical parameters on the frequency spectra.

4. Dispersion relation and numerical solution

Using the method of separation of variables, we search for solutions of $\Phi^j(r, z)$ on the basis of cylindrical harmonics. Solutions of (28) satisfying conditions (30) may be written as follows:

$$\rho^j \Phi^j = A_0^j(r^m + \alpha_0^j r^{-m}) + \rho^j \omega^2 \sum_{k=1}^{\infty} A_k^j \mathscr{R}^j(\beta_k r)\, \mathscr{Z}^j(\mu_k z), \tag{31}$$

where ω and A_k^j are unknown constants which must be determined from the analysis. Functionals $\mathscr{R}^j(\beta_k r)$ and $\mathscr{Z}^j(\mu_k z)$, which hereinafter are to be written $\mathscr{R}_k^j$ and $\mathscr{Z}_k^j$ for brevity, have different forms depending on the problem under consideration. Constants β_k and μ_k are related by

$$\beta_k^j = \mu_k^j(|1-\lambda^2|)^{\frac{1}{2}} \tag{32}$$

and they must be calculated together with α_0^j taking into account conditions (30). Depending on the meniscus geometry, one may use a different series expansion (see Appendix C). Substituting the appropriate expansion in (29) one arrives at a homogeneous system of an infinite number of algebraic equations:

$$\omega^2(1-\lambda^2)\left[\sum_{k=1}^{\infty}(A_k^{\mathrm{o}}\rho^{\mathrm{o}}\mathscr{E}_{k,q}^{\mathrm{o}} - A_k^{\mathrm{i}}\rho^{\mathrm{i}}\mathscr{E}_{k,q}^{\mathrm{i}}) + A_0^{\mathrm{o}}\rho^{\mathrm{o}}\mathscr{G}_q^{\mathrm{o}} - A_0^{\mathrm{i}}\rho^{\mathrm{i}}\mathscr{G}_q^{\mathrm{i}}\right]$$

$$-l_q\left\{\sum_{k=1}^{\infty}A_k^j[\mathscr{H}_{k,q}^j - (1-\lambda^2)\mathscr{M}_{k,q}^j] - A_0^j m(1-\lambda)\mathscr{N}_q^j\right\} = 0, \quad j = \mathrm{i}, \mathrm{o}; \quad q = 1, 2, \ldots, \tag{33}$$

where

$$\mathscr{E}^j_{k,q} = \int_0^{s_0} \mathscr{R}^j_k \mathscr{Z}^j_k \zeta^*_q F_e \, ds, \tag{34}$$

$$\mathscr{G}^j_q = \int_0^{s_0} \mathscr{F}_1 \zeta^*_q F_e \, ds, \tag{35}$$

$$\mathscr{H}^j_{k,q} = \int_0^{s_0} \left(\frac{d\mathscr{R}^j_k}{dr} - \frac{\lambda m}{r} \mathscr{R}^j_k \right) \mathscr{Z}^j_k \cos(\Theta_e) \zeta^*_q F_e \, ds, \tag{36}$$

$$\mathscr{M}^j_{k,q} = \int_0^{s_0} \frac{d\mathscr{Z}^j_k}{dz} \mathscr{R}^j_k \sin(\Theta_e) \zeta^*_q F_e \, ds, \tag{37}$$

$$\mathscr{N}^j_q = \int_0^{s_0} \mathscr{F}_2 \sin(\Theta_e) \zeta^*_q \, ds \tag{38}$$

and

$$\mathscr{F}_1 = \begin{cases} F_e^m + \alpha_0^j F_e^{-m} & \text{liquid bridges,} \\ 1 \quad \text{if} \quad m = 0 & \\ 0 \quad \text{if} \quad m \neq 0 & \text{drops,} \end{cases} \tag{39}$$

$$\mathscr{F}_2 = \begin{cases} F_e^m - \dfrac{(1+\lambda)}{(1-\lambda)} \alpha_0^j F_e^{-m} & \text{liquid bridges,} \\ 0 & \text{drops.} \end{cases} \tag{40}$$

In general, when $m = 0$, one has

$$\mathscr{G}^i_q \equiv \mathscr{G}^o_q = \int_0^{s_0} \zeta^*_q F_e \, ds$$

Moreover, the constant-volume condition (22) results in

$$\sum_{k=1}^{\infty} (A^o_k \rho^o E^o_k - A^i_k \rho_i E^i_k) + (A^o_0 \rho^o - A^i_0 \rho^i) G^i = 0, \tag{41}$$

where

$$E^j_k = \sum_{q=1}^{\infty} \frac{D_q \mathscr{E}^j_{k,q}}{l_q}, \tag{42}$$

$$G^j = \sum_{q=1}^{\infty} \frac{D_q \mathscr{G}^j_q}{l_q}, \tag{43}$$

and

$$D_q = \frac{\int_0^{s_0} \zeta^*_q F_e \, ds}{\int_0^{s_0} \{\zeta^*_q\}^2 F_e \, ds}. \tag{44}$$

The requirement of the existence of a non-trivial solution for system (33) yields the natural frequencies ω and the eigenvectors $\{A^j_k\}_{k=0,1,\ldots;j=i,o}$.

From the point of view of the numerical resolution, one should search for solutions of Φ^j in a discrete generalized Fourier basis $\{\Phi^j_k(r,z)\}_{k=1,2,\ldots,N^j}$, which represents an approach to the actual basis $\{\Phi^j_k(r,z)_{k=1,2,\ldots,\infty}$. Thus, the infinite series in (33) and (41) must be truncated after an appropriate N^j-term. Hence, the $N^i + N^o + 2$ unknowns

$$\{A^j_k\}_{k=0,1,\ldots,N^j}, \quad j = i, o \quad \text{for } m \neq 0$$

and the $N^i + N^o + 1$ unknowns

$$\{[A^j_k]_{k=1,\ldots,N^j,\ j=i,o},\ (A^o_0 \rho^o - A^i_0 \rho^i)\} \quad \text{if} \quad m = 0$$

constitute a discrete dimension eigenvector for the problem, ω being its corresponding eigenvalue. Consequently, if $m \neq 0$ only the first N^j+1 equations of the system (33) (if $m = 0$, only the first N^j-equations plus (41)) should be taken into account. Finally, an approximate dispersion relation is supplied from the vanishing of the determinant of the homogeneous finite algebraic system. In other words, if system (33) is written as

$$[M^j_{k,q}(\omega)]\{A^j_k\} = 0, \tag{45}$$

the eigenvalues ω are the roots of the function given by the determinant of the truncated system (45):

$$F(\omega) = |M^j_{k,q}(\omega)|, \tag{46}$$

In general, the function $F(\omega)$ should be written

$$\left.\begin{aligned} F &\equiv F(\omega, m, n, N^{\mathrm{i}}, N^{\mathrm{o}}, W, B, \rho^{\mathrm{o}}/\rho^{\mathrm{i}}, V, R_1, R_2, H_0) \quad \text{floating zones} \\ F &\equiv F(\omega, m, n, N^{\mathrm{i}}, N^{\mathrm{o}}, W, B, \rho^{\mathrm{o}}/\rho^{\mathrm{i}}, V, H_0, H_1, H_2) \quad \text{captive drops} \end{aligned}\right\} \tag{47}$$

but, the sake of brevity, we shall simply write $F(\omega)$.

For accuracy, if one is considering the N first natural frequencies of the spectrum, N^j should in general be much greater than N. A numerical analysis of the convergence and sensibility of the number N can be found in Gañan & Barrero (1990) for $\Omega = 0$. As a general remark, for most cases we have found the convergence to be very fast within the limits of application of the method. If $N^j > 5$, the typical error for the first frequency is of $O(0.1\%)$. However, in the case of axisymmetric modes of liquid bridges, a number of retained terms $N^j > 10$ is required for the same accuracy. In the following section we outline how the rotation affects the convergence. On the other hand, in the presence of rotation ($\lambda \neq 0$) the solution of the dispersion relation cannot be done by standard methods as in the case of $\lambda = 0$ (Gañán & Barrero 1990). Thus, trial-and-error or bisection methods should be used with the aid of a Newton–Raphson method in the neighbourhood of the eigenvalue that we are seeking.

5. Numerical results

In the following, we will present the results of the numerical analysis corresponding to $\lambda \neq 0$ (with rotation). The influence of gravity, density of the fluids and geometrical parameters for the case $\lambda = 0$ have been considered elsewhere (Gañán & Barrero 1990).

To analyse the role that rotation plays in the natural frequency spectra of captive drops, in the following we will discuss a set of examples corresponding to selected combinations of density ratios and geometrical parameters for continuous ranges of Bond and Weber numbers. Although the character of equation (28) does not put a limit on the generality of equations (33) and (41), from the point of view of their numerical solution in the hyperbolic regime, it has to be pointed out that the hyperbolic frequency spectrum is dense over $(0, 2\Omega)$ (Myshkis *et al.* 1987). This is manifested by the fact that in the interval $\omega \in (0, 2\Omega)$ the oscillating character of the function $F(\omega)$ in (47) increases (the number of roots increases) and its amplitude decreases as the number of retained terms N^j in the series increases. We have numerically found that $F(\omega)$ uniformly tends to zero in the interval $\omega \in (0, 2\Omega)$ as $N^j \to \infty$. Consequently, the convergence cannot be improved by increasing N^j because the difference between the value of a certain root $\omega_{m,n}$ for certain N^j and the value for N^j+1 becomes of the same order as the distance between two roots of $F(\omega)$. In this case it is useful to define the eigenvalues of the problem as the inverse of the oscillation frequencies (Greenspan 1968).

However, the inviscid assumption becomes invalid for very slow oscillations

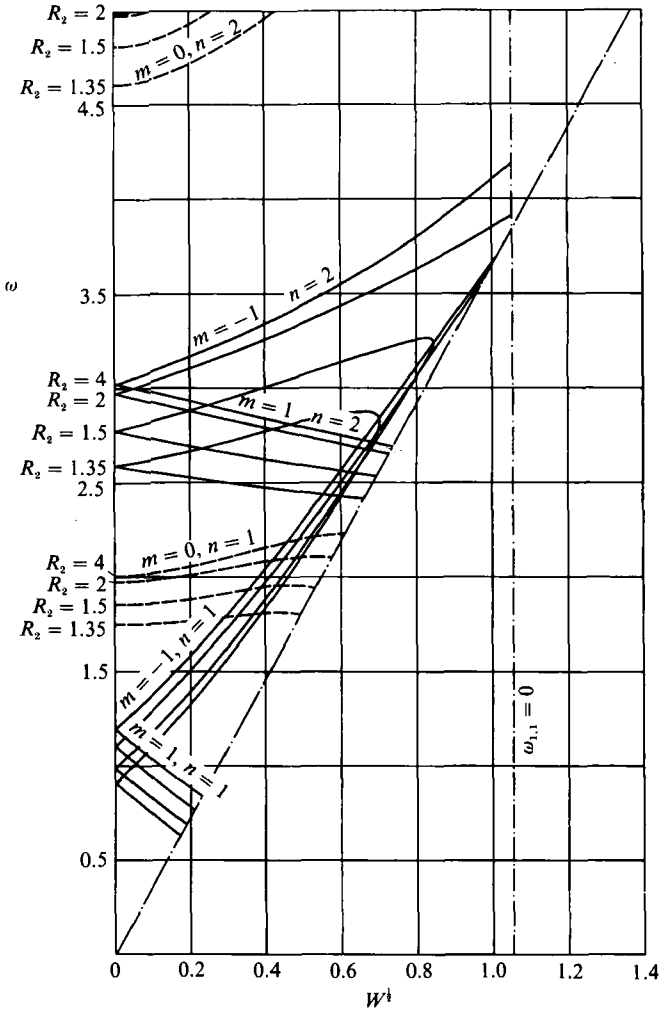

FIGURE 4. First two frequencies for $m = 0$ and $m = \pm 1$ versus the Weber number W of a liquid bridge between equal disks, slenderness $H_0 = 2.5$, volume $V = 2.5\pi$, Bond number $B = 1$, and surrounded by an outer medium of density $\rho^o = 0.35$, for different values of the vessel radius R_2.

(hyperbolic regime) and the physical application of the model is less plausible. For that reason we have restricted our analysis to finding the frequencies and oscillation modes of surface waves (elliptic regime). This study is equivalent to analysing the roots of the function (47). In what follows we describe in detail the structure of the roots of (47) for a few values of the vector $(V, R_1, R_2, \rho^o/\rho^i, H_0)$ and the first and second wavenumbers in order to illustrate the power of the present method. Further analytical effort would be required to define a proper solution scheme to determine the hyperbolic spectrum.

5.1. *Bridges or floating zones*

Figure 4 shows the first and second frequencies of the axisymmetric ($m = 0$) and asymmetric ($m = 1$, $m = -1$) modes of a liquid bridge between two equal-diameter disks, of slenderness $H_0 = 2.5$, volume $V = 2.5\pi$, Bond number $B = 1$, and

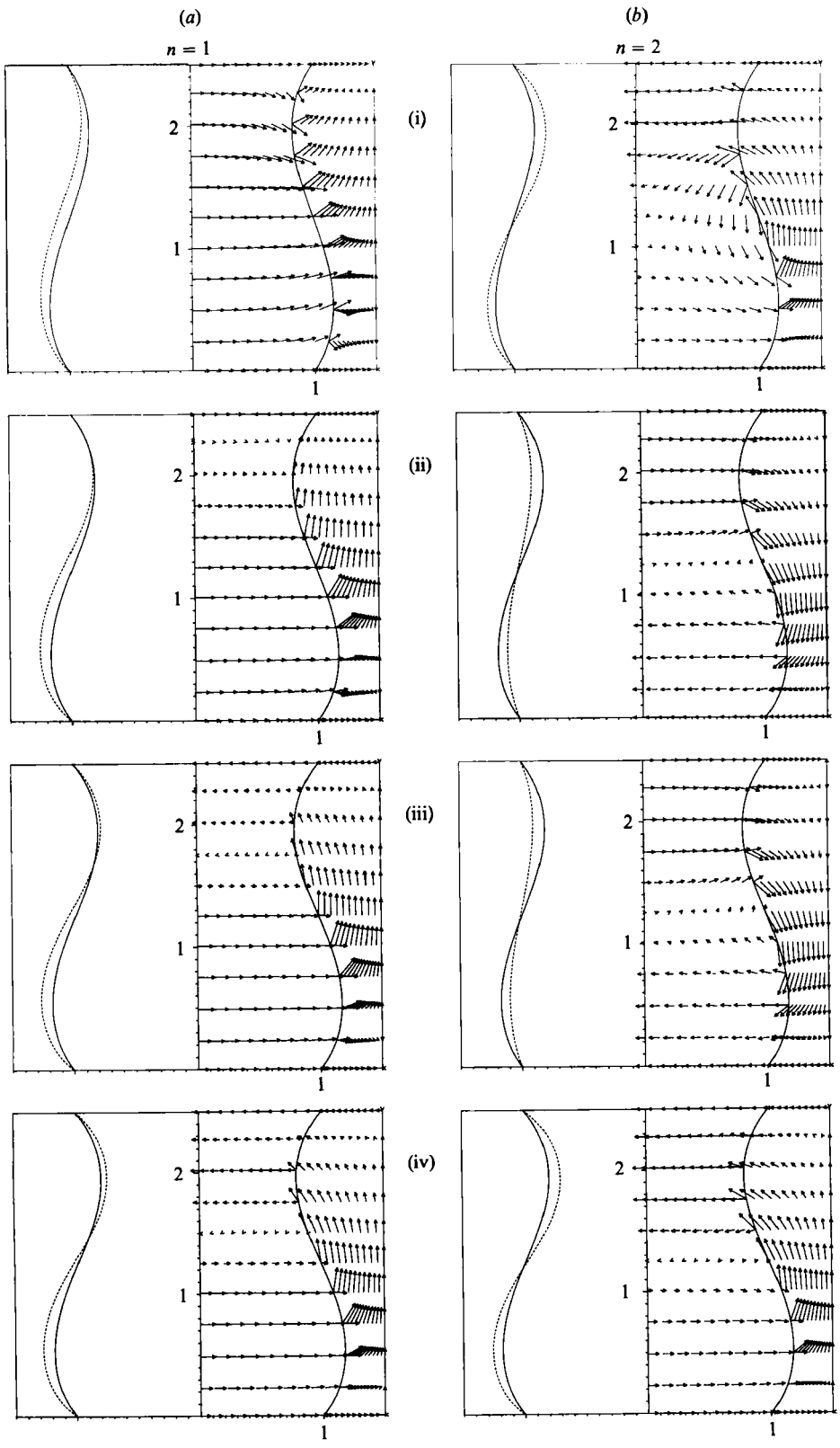

FIGURE 5. Surface deformation and velocity fields for (*a*) the first and (*b*) the second oscillation modes for $m = -1$ for the liquid bridge of figure 4, for (i) $W^{\frac{1}{2}} = 0.3$, (ii) $W^{\frac{1}{2}} = 0.65$, (iii) $W^{\frac{1}{2}} = 0.75$, and (iv) $W^{\frac{1}{2}} = 0.8$.

surrounded by an outer fluid of density $\rho^o = 0.35$, for different values of the vessel radius R_2. The vertical dashed-dot line represents the maximum Weber number (or the stability limit) for this particular bridge. It should be stressed that the equilibrium problem (i.e. the equilibrium shape) has to be solved for each W. In the case of this particular bridge, the limit is first reached by an asymmetric forward mode ($m = 1$). The character of the stability limit depends on the values of H_0, R_1, and V (Vega & Perales 1983).

The sloping dashed-dot line is the interface between the elliptic ($\omega^2 > 4W/(\rho^i - \rho^o)$) and the hyperbolic ($\omega^2 < 4W/(\rho^i - \rho^o)$) regions. In the elliptic region, one may observe the splitting of frequencies corresponding to the forward ($m = 1$) and backward ($m = -1$) modes, while both have the same value for non-rotating menisci. Furthermore, the frequency of the first mode decreases for $m = 1$, and increases for $m = -1$ as W increases. Indeed, this effect is a characteristic of the first modes $m = 1$ and $m = -1$ for all captive menisci, as will be shown in our results. This led Myshkis *et al.* to outline as a general characteristic that $\omega_{m,n} < \omega_{-m,n}$ (Myshkis *et al.* 1987, pp. 329–330), which in general is not correct, as will be shown for the case of $\rho^i < \rho^o$ and $m = \pm 2$. On the other hand, the first and second frequency of the axisymmetric ($m = 0$) modes increase as W increases until one of them reaches either the straight line $\omega = 2\Omega$ or the stability limit.

One of the most interesting features discovered for the elliptic spectrum is that, for a certain azimuthal wavenumber m and increasing rotation speed, two different modes eventually *collapse* to a single one. Above the value of the rotation speed for which this happens, both disappear from the elliptic spectrum (see figure 4 for the first and second $m = -1$ modes and $R_2 \leqslant 1.5$).

This phenomenon is described in figure 5(a, b) where the surface deformation and velocity fields corresponding to the first and second backward modes $m = -1$ for $W^{\frac{1}{2}} = 0.3$, 0.65, 0.75, and 0.8, and $R_2 = 1.5$ are represented. The right-hand part of each graph shows the instant of minimum amplitude of the interface motion (maximum amplitude of the velocity), and the left-hand part shows the interface at a time $\pi/2\omega$ later. As a consequence of the ideal liquid approximation, observe that through the interface the tangential velocity is not conserved. This analysis is equivalent to considering the interface as a thin film of thickness

$$\delta \sim (\nu^2 \tilde{\rho} \tilde{R}_0^3 \sigma^{-1})^{\frac{1}{2}} \ll \tilde{R}_0,$$

disregarding small shear stresses inside this film, which are responsible for the continuity of the velocity vectors through the interface.

For W ranging from $W^{\frac{1}{2}} = 0$ to ~ 0.65 (see figure 5a, b), there are no other nodes on the interface profile apart from the upper and lower contact line. However, for values larger than $W^{\frac{1}{2}} \sim 0.65$ a *new node* appears and moves from the upper contact line downwards along the profile as W is increased. Both interface deformation and velocity fields for the $m = -1$ $n = 1$ mode become very similar to those for the next mode ($m = -1$, $n = 2$). On the other hand, the $m = -1$, $n = 2$ mode changes only slightly as W increases (see figure 5 for $W^{\frac{1}{2}} = 0.75$ and 0.8). We have found that the radius R_2 of the cylindrical container determines the occurrence of this phenomenon in such a manner that it does not take place for values of R_2 larger than ~ 1.84 for this particular liquid bridge. Figure 6 shows how the first backwards mode is modified for this bridge when R_2 increases from 1.5 to 2 ($W = 0.8$). Similar behaviour may be observed for most of the capillary menisci under rotation as a rigid body inside a *cylindrical* container.

Figure 7 represents the first axisymmetric, and the first and second asymmetric

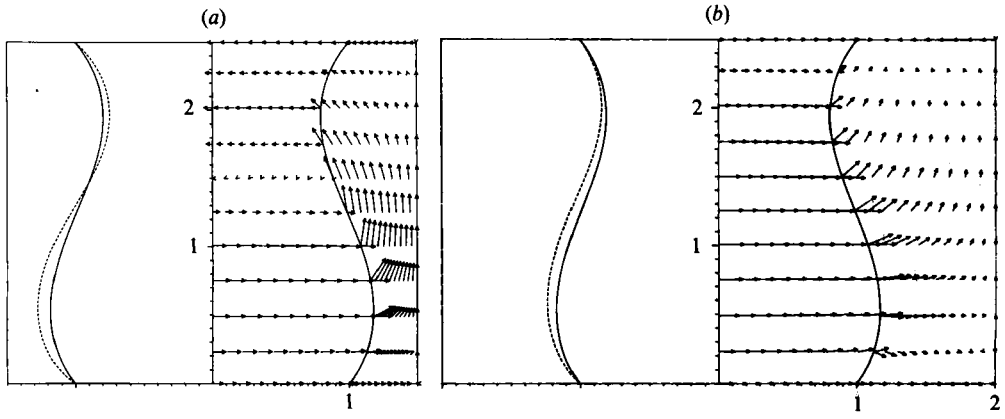

FIGURE 6. Surface deformation and velocity fields for the first backwards mode ($m = -1$, $n = 1$) of the same liquid bridge of figures 4 and 5 for $W = 0.8$: (*a*) $R_2 = 1.5$, (*b*) $R_2 = 2$.

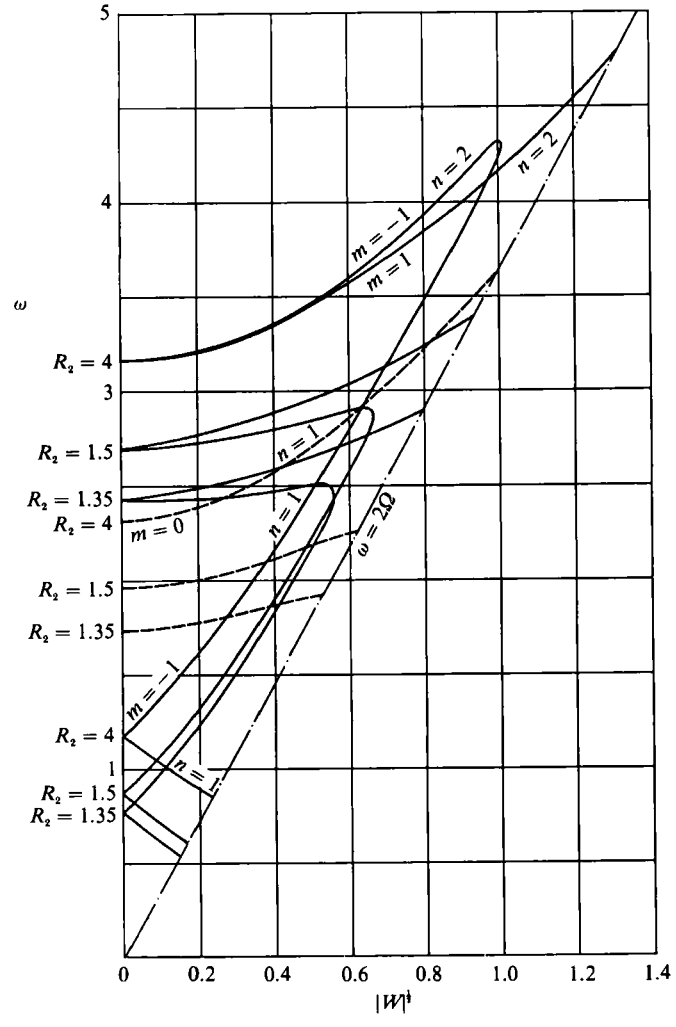

FIGURE 7. First frequency for $m = 0$, and first two frequencies for $m = \pm 1$ versus the Weber number W, for different values of R_2 of a liquid bridge with the same parameters as figure 4 except that $\rho^o = 0.65$.

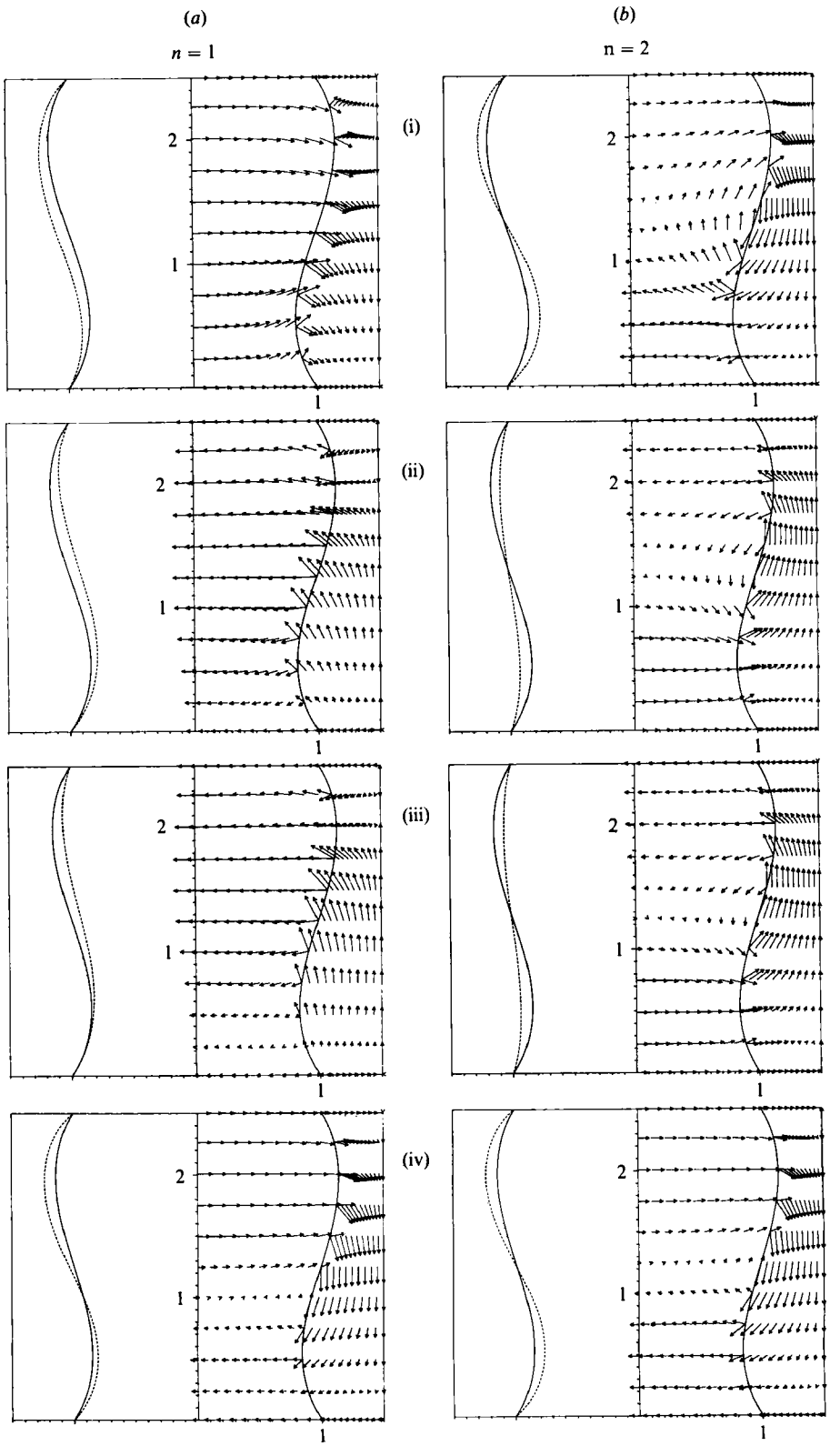
(a)
n = 1
(b)
n = 2
(i)
(ii)
(iii)
(iv)
2
1
1

($n = 1, 2, m = -1, 1$) frequencies of a liquid bridge with the same volume V, height H_0, and upper radius R_1 as in the former case (see figure 4), but in the present case the inner density ($\rho^i = 0.35$) is lower than the outer one (the meniscus acts as a 'bubble'). Here, the effect of rotation is to stabilize the meniscus. All the oscillation frequencies, except that corresponding to the $m = 1, n = 1$ mode, increase as $|W|$ increases. In this case, note that frequencies $\omega_{1,1}$ not only increase with $|W|$, but also $\omega_{1,2} > \omega_{-1,2}$, which refutes the general conclusion drawn by Myshkis *et al.* from their partial results (a meniscus inside a tube: they drew as a general conclusion (pp. 329–330) that for the surface waves, $\omega^{\text{backward}} > \omega^{\text{forward}} (> 2\Omega)$). Moreover, when $\rho^i < \rho^o$, no stability limit is reached for any real value of $|W|$, and the elliptic spectrum appears the same as the one in figure 4 for $R_2 \leqslant 1.5$, but in the present case the collapse of modes $m = -1$, $n = 1$ and $m = -1$, $n = 2$ takes place for any value of R_2. Figure 8 (a, b) shows the velocity fields and interface deformations corresponding to the first and second backward modes ($m = -1$) of this liquid bridge, $R_2 = 1.5$, and different values of the Weber number. Note the similarity between the first and second modes as $|W|$ approaches $|W^*|^{\frac{1}{2}} \sim 0.66$.

From the numerical point of view, the convergence is excellent in the case $m = \pm 1$. For $N = 3$, an error $\epsilon = [(\omega(N) - \omega(N-1))/\omega(N)] \times 100 = 0.2\%$ can be achieved for the first and second frequencies ($n = 1$, $n = 2$), decreasing to $\epsilon = 0.005\%$ for $N = 9$. As suggested in Appendix C, this convergence improves as W increases. Nevertheless, the same accuracy for the axisymmetric case $m = 0$ requires $N = 7$ and $N = 20$ terms in the series, respectively. This may be caused by the existence of a solution $\Phi^j =$ const., which in the present method is expanded in series, causing a deterioration in the convergence.

5.2. *Captive drops or bubbles*

The influence of rotation on the asymmetric oscillations $m = 1$ and $m = -1$ of a non-surrounded captive drop in the absence of gravity and in contact with a circular flat support (disk) is analysed. The contact line is fixed at the edge of the disk. If the frequencies $\omega_{1,1}$ and $\omega_{-1,1}$, and the rotation speed Ω (which is $|W|^{\frac{1}{2}}$ in this case) are normalized with the frequency of the same drop in the absence of rotation $\omega^0_{1,1}$, one finds that all the curves $\omega_{\pm 1,1}(\Omega)$ collapse for values of the drop volume ranging from $V \approx 0.4$ to ≈ 50. In figure 9 we show the resulting universal plot of the first frequencies $\omega_{\pm 1,1}/\omega^0_{1,1}$ versus the rotation speed $\Omega/\omega^0_{1,1}$, where $\omega^0_{1,1}$ is the first transverse frequency of the drop in the absence of rotation. The following general formula may be derived for the first frequency $m = 1$ and $m = -1$ of a rotating liquid captive drop with $B = 0$:

$$\omega_{\pm 1,1} = \omega^0_{\pm 1,1} \mp \Omega. \tag{48}$$

This result was found using about 6–7 eigenfunctions. All the computed frequencies lay on a single line within an error $\pm 0.5\%$.

The influence on the oscillations of a captive drop of both the isorotational and the gravitational fields has been analysed in the case of $V = 2.3$. Figure 10 shows the first frequency of the axisymmetric modes $m = 0$ for different values of the Bond number B. The dashed-dot represents the stability limit (due to the first non-symmetric $m = 1$ mode). Observe that, although the oscillation frequency decreases when B increases, the stabilization effect due to rotation increases (the slope of the curve $\omega(\Omega)$ increases). On the other hand, the slope of $\omega_{0,n}$ tends to 0 when $\Omega \to 0$. Note that

FIGURE 8. Velocity and deformation fields for (a) the first and (b) the second oscillation modes for $m = -1$ for the liquid bridge of figure 7 for (i) $W = 0$, (ii) $|W|^{\frac{1}{2}} = 0.3$, (iii) $|W|^{\frac{1}{2}} = 0.5$, and (iv) $|W|^{\frac{1}{2}} = 0.65$.

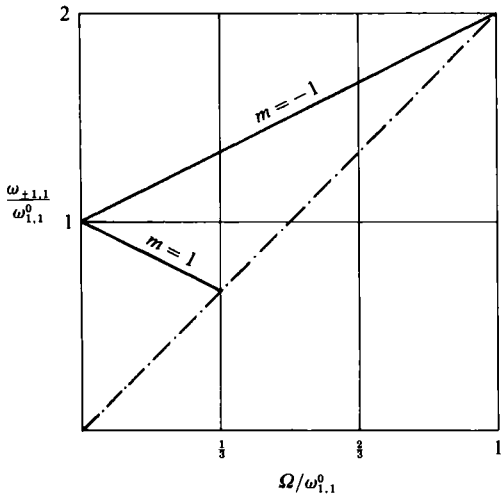

FIGURE 9. First frequency for $m = 1$ and $m = -1$ of a captive rotating liquid drop with $B = 0$ and $\rho^o = 0$, versus the rotation speed Ω. Results are given in general form by scaling the graphics with the first oscillation frequency $m = 1$ of the drop for $\Omega = 0$.

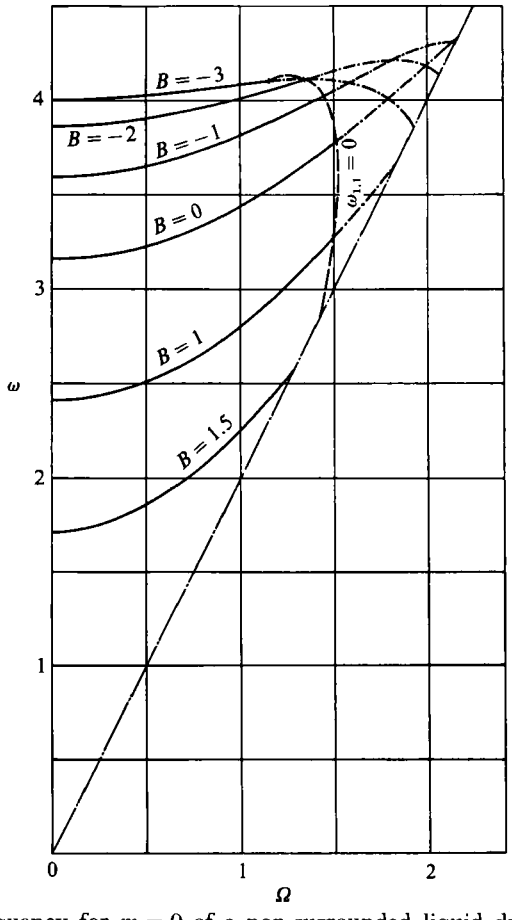

FIGURE 10. First frequency for $m = 0$ of a non-surrounded liquid drop of volume $V = 2.3$, for different values of the Bond number B. The stability limit is represented as a dashed-dot line. For this volume, the stability limit is reached by the axisymmetric mode $m = 0$.

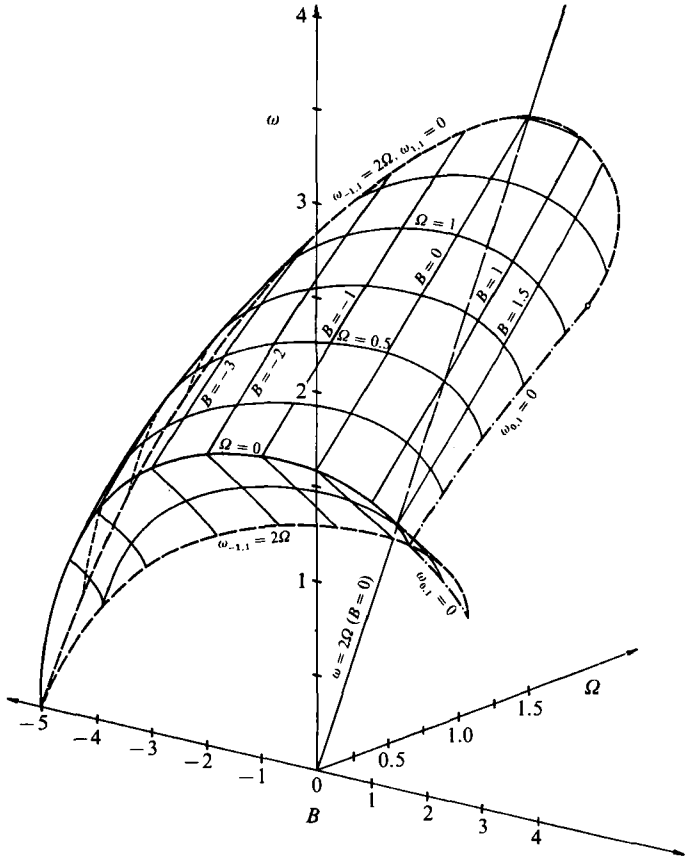

FIGURE 11. First frequencies for $m = 1$ and $m = -1$ of the drop in figure 10 versus the Bond number B and rotation speed Ω ($\Omega = W^{\frac{1}{2}}$ because $\rho^{o} = 0$). The transition to the hyperbolic regime is represented by dashed lines, and the stability limit $\omega_{0,1} = 0$ is given by dot-dashed lines.

the equilibrium shape given by (A 1)–(A 3) (see Appendix A), the interface perturbation ζ_q^* from (17), and the velocity fields expressed in (C 9)–(C 16) (see Appendix C) are functions of Ω^2 when $m = 0$.

In figure 11 the non-symmetric $m = 1$ and $m = -1$ modes of the same drop are represented as a function of both B and W ($W \equiv \Omega$ in this case). It is of interest to notice that for low and negative Bond numbers, the lower value of the Weber number given by the stability criterion corresponds to the first $m = 1$ mode, and for positive higher values of B ($B > 1.78$), it corresponds to the first axisymmetric $m = 0$ mode. For a given B, the stabilization effect due to rotation can be qualitatively estimated from the slope of the curve $\omega_{0,1}(\Omega)$.

The physical explanation of this phenomenon is not difficult if one keeps in mind the distortion of the equilibrium shape due to the Bond number (concentrating the liquid around the z-axis when positive, and allowing it to spread when negative) and the Weber number (pushing mass away from the z-axis when positive, or the opposite when negative). When both effects contribute to spread the liquid away from the axis of rotation, the most 'dangerous' mode of oscillation (the one which determines the stability limit) is the non-symmetric $m = 1$ case. If a characteristic radius R^* is defined from the drop volume $R^* = (3V/4\pi)^{\frac{1}{3}}$, one has that the 'flatter' the drop, that

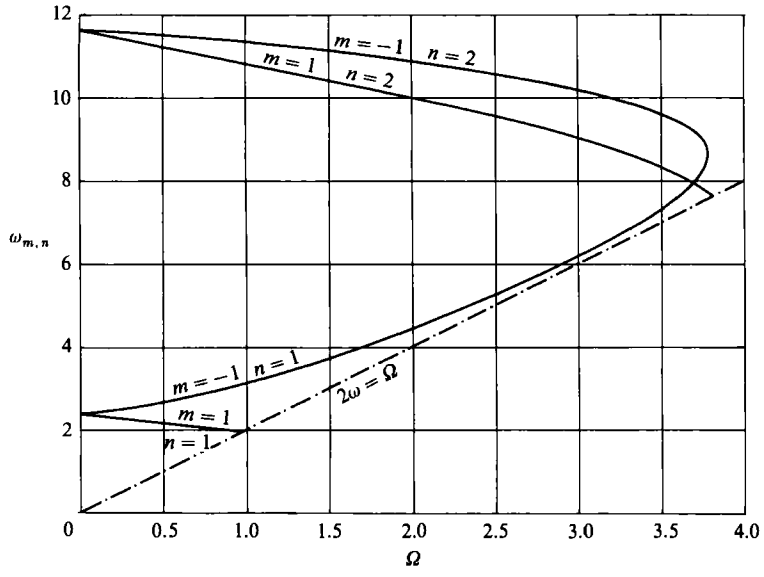

FIGURE 12. First and second frequencies $m = 1$ and $m = -1$ for the meniscus described in Myshkis *et al.* (1987, p. 378) for $\alpha = 60°$, versus the rotation speed Ω. The results of Myshkis *et al.* are extended over larger values of Ω and the same phenomena as in liquid bridge are found for the first and second $m = -1$ modes.

is, the smaller R^*, the more dangerous (the more unstable) the $m = 1$ mode becomes. If the drop is flat enough, the most unstable mode, even in the absence of rotation, is $m = 1$ whatever the value of B. Nevertheless, the effect of gravity is the opposite, stretching the drop along the z-axis when it is voluminous and, therefore, the dangerous mode depends on the value of R^* (for a thorough review of the equilibrium and stability of axisymmetric drops, see Myshkis *et al.* 1987).

Figure 12 shows the first and second frequencies $m = 1$ and $m = -1$ of the meniscus described in Myshkis *et al.* (pp. 378) for $\alpha = 60°$, versus the rotation speed Ω. It should be noticed that there is now a slip condition in the contact line. Thus, the boundary condition for the perturbation of the interface becomes

$$\left.\frac{\mathrm{d}\zeta}{\mathrm{d}s}\right|_{s=s_0} = 0. \tag{49}$$

Here, we have extended the results of Myshkis *et al.* over larger values of Ω and we have found for the first and second modes $m = -1$ the same phenomenon as in liquid bridges: both modes suddenly become a single one for a certain value of the rotation speed Ω^*, and then both disappear for larger values of Ω. The excellent fit between Myshkis *et al.*'s results and ours is to be expected since we have both used the separation of variables method to solve the problem.

Finally, in the case of drops inside a tube, the numerical integration schemes should be refined in order to ensure convergence and accuracy of the results. Owing to the exponential functions that appear in (31) (also see Appendix C), the larger the rotation parameter λ, the more difficult the convergence becomes as the number of eigenfunctions needed increases.

6. Summary and discussion of the results

An analytical spectral method to determine the natural frequencies and the corresponding normal modes of inviscid liquid captive drops or bubbles (pendant or sessile drops, and liquid bridges), surrounded by an outer liquid or gas, under the influence of both gravitational and isorotational fields, has been developed. The method uses a small-disturbance approach and the normal mode decomposition to linearize and reduce the inviscid Navier–Stokes equations and boundary conditions to an eigenvalue problem. The solution of the second-order differential equation of the interface motion is expressed using the Green function method. Both the Green function and normal velocities at the interface are expanded in the orthogonal functional space generated by the Sturm–Liouville problem associated with the homogeneous part of the interface equation. The analysis is then reduced to three sets of an infinite number of algebraic equations that are numerically solved using appropriate truncation.

We report numerical results taking into account the influence of rotation on the small oscillations of liquid captive drops. In agreement with the study of Myshkis *et al.* (1987), the current study shows that the frequency spectrum $\{\omega_{m,n}\}$ is split into two sets corresponding to the elliptic ($\omega > 2\Omega$) and the hyperbolic ($\omega < 2\Omega$) regimes. The structure of the elliptic frequency spectrum as a function of the Weber number for some liquid bridges and drops has been described in detail for low azimuthal ($m = 0, \pm 1$) and meridional ($n = 0, 1, 2$) wavenumbers.

For liquid bridges, some general results can be summarized as follows:

(*a*) Oscillation frequencies decrease as the radius R_2 of the vessel that contains the liquid bridge and the outer liquid decreases.

(*b*) When $\rho^i < \rho^o$ and $B \neq 0$, a collapse of the first and second ($n = 1$ and $n = 2$) backward modes $m = -1$ occurs for certain value W^* of the Weber number, which depends on R_2. Both modes disappear from the elliptic spectrum for $|W| > |W^*|$.

(*c*) When $\rho^i > \rho^o$, three different scenarios are found: (i) for $R_2 < R_2^*$, where R_2^* is a certain limiting value of the vessel radius that can be numerically found, the collapse of the first and second backward ($m = -1$) modes takes place for a value of W which depends on R_2. (ii) The bridge reaches its stability limit before the collapse takes place ($R_2 > R_2^*$). (iii) The curve $\omega_{-1,1}(|W|^{\frac{1}{2}})$ ends up on the line $\omega^2 = 4W/(\rho^i - \rho^o)$, which establishes the limit between the elliptic and the hyperbolic spectra ($R_2 > R_2^*$).

For captive drops, the following conclusions may be outlined:

(*a*) For non-surrounded rotating liquid captive drops supported in a disk of radius $R_0 = 1$, in the absence of rotation, there is a general relation for the frequencies of the first forward and backward modes ($m = \pm 1$):

$$\omega_{\pm 1,1}(\Omega) = \omega_{1,1}^0 \mp \Omega$$

where $\omega_{1,1}^0$ is the frequency of the same drop in the absence of rotation.

(*b*) When the inner region of the meniscus is occupied by a fluid which is less dense than the one that fills the rest of the space, the same phenomenon described for liquid bridges occurs, i.e. the collapse of the first and second backward modes. For the opposite density ratio between the inner and outer fluid, the phenomenon may take place if the stability limit is not reached first.

In general, the isorotational field was found to stabilize the meniscus when $\rho^i < \rho^o$. However, when $\rho^i > \rho^o$ this effect may reverse depending on the geometry of the meniscus, the Bond number and the oscillation mode under consideration. The examples analysed in §5 for both liquid bridges and drops illustrate the influence of

the Bond and Weber numbers, boundary conditions and densities of both inner and outer fluids. Furthermore, the oscillation modes corresponding to the lower wavenumbers are the most affected by the isorotational field because the characteristic times of rotation and oscillation are of the same order, which means that the oscillation frequencies and corresponding modes are less affected by rotation for large wavenumbers m and n. Finally, the convergence of the method when using separation of variables in cylindrical coordinates, which was shown in Gañán & Barrero (1990) in the absence of rotation, is improved with rotation in the case of liquid bridges (see Appendix C). In this case, the convergence limits depend on the Bond number, the volume V and the slenderness H_0. However, for captive drops the convergence deteriorates as Ω increases, and the limits of convergence depend strongly on the rotation speed.

Further insight is required on the properties of the hyperbolic spectrum in order to complete the description of the small oscillations of captive rotating liquid drops and bubbles.

This work, partially supported by the Consejería de Educación de la Junta de Andalucía, has been conducted at the Universidad de Sevilla, Spain, in partial fulfilment of the requirements for my doctoral degree. I am particularly indebted to Professor Barrero from the Universidad de Sevilla (Spain) for his encouragement, advice, criticism and support throughout this work. It is also a pleasure to thank Professor Lasheras from the University of California, San Diego for all his helpful suggestions.

Appendix A

In terms of the s-coordinate and the slope angle of the equilibrium profile Θ_e, the equilibrium coordinates $r = F_e(s)$ and $z = Z_e(s)$ are given by

$$\frac{\mathrm{d}\Theta_e}{\mathrm{d}s} = P_0 - BZ_e - \frac{\sin\Theta_e}{F_e} + \tfrac{1}{2}WF_e^2, \tag{A 1}$$

$$\frac{\mathrm{d}F_e}{\mathrm{d}s} = \cos\Theta_e, \quad \frac{\mathrm{d}Z_e}{\mathrm{d}s} = \sin\Theta_e, \quad \frac{\mathrm{d}F_e}{\mathrm{d}z} = \frac{\cos\Theta_e}{\sin\Theta_e} \tag{A 2)–(A 4}$$

and

$$1 + F_{e_z}^2 = \sin^{-2}\Theta_e. \tag{A 5}$$

Taking into account that

$$\frac{\mathrm{d}\eta}{\mathrm{d}z} = \frac{\mathrm{d}\eta}{\mathrm{d}s}\frac{1}{\sin\Theta_e} \tag{A 6}$$

and

$$\frac{\mathrm{d}}{\mathrm{d}z}\left[\frac{F_e\eta_z}{(1+F_{e_z}^2)^{\frac{3}{2}}}\right] = \frac{1}{\sin\Theta_e}\frac{\mathrm{d}}{\mathrm{d}s}\left(F_e\sin^2\Theta_e\frac{\mathrm{d}\eta}{\mathrm{d}s}\right)$$

$$= \sin^{-1}\Theta_e\left(F_e\sin^2\Theta_e\frac{\mathrm{d}^2\eta}{\mathrm{d}s^2} + \sin^2\Theta_e\frac{\mathrm{d}\eta}{\mathrm{d}s}\frac{\mathrm{d}F_e}{\mathrm{d}s} + 2\cos\Theta_e\sin\Theta_e\frac{\mathrm{d}\Theta_e}{\mathrm{d}s}F_e\frac{\mathrm{d}\eta}{\mathrm{d}s}\right), \tag{A 7}$$

and introducing expressions (A 4), (A 5), (A 6), and (A 7) into (8), one arrives at

$$\frac{\mathrm{d}^2\eta}{\mathrm{d}s^2}\sin\Theta_e + 2\cos\Theta_e\frac{\mathrm{d}\Theta_e}{\mathrm{d}s}\frac{\mathrm{d}\eta}{\mathrm{d}s} + \sin\Theta_e\cos\Theta_e F_e^{-1}\frac{\mathrm{d}\eta}{\mathrm{d}s}$$

$$+ \eta(1-m^2)F_e^{-2}\sin\theta_e + WF_e\eta = \rho^o\Phi^o - \rho^i\Phi^i. \tag{A 8}$$

Finally, defining

$$\zeta(s) = \eta(Z_e(s)) \sin \Theta_e(s), \tag{A 9}$$

and substituting it into (A 8) we obtain (16).

It is of interest to notice that (8) may also be written in terms of the r-coordinate and yields (16) again when it is written on the s-coordinate along the drop profile. If we specify the interface position in the form $f(r, \varphi, z, t) \equiv Z(r, \varphi, t) - z$, we can write the perturbations as

$$Z(r, \varphi, t) = Z_e(z) + \sum_{m=0}^{\infty} \sum_{n=1}^{\infty} \gamma_{m,n}(r)\, e^{i(m\varphi - \omega_{m,n} t)}. \tag{A 10}$$

The second-order problem on the r-coordinate is given by

$$r^{-1}[r\gamma_r(1+Z_{e_r}^2)^{-\frac{3}{2}}]_r + \gamma[B - m^2 r^{-2}(1+Z_{e_r}^2)^{-\frac{1}{2}}] = \rho^i \Phi^i(r, Z_e(r)) - \rho^o \Phi^o(r, Z_e(r)), \tag{A 11}$$

where subscript r stands for the r-derivative; the boundary conditions are

(a) bridges

$$\gamma(0) = 0, \quad \gamma(1) = 0; \tag{A 12}$$

(b) drops

$$\gamma(R_1) = 0, \quad \mathrm{d}\gamma/\mathrm{d}s|_{r=0} = 0, \tag{A 13}$$

for the axisymmetric mode ($m = 0$), or

$$\gamma(0) = 0, \quad \gamma(1) = 0, \tag{A 14}$$

for non-symmetric modes ($m > 0$).

The volume condition reads

$$\int_0^{R_1} r\gamma(r)\, \mathrm{d}r = 0. \tag{A 15}$$

A similar manipulation of (A 11) yields

$$\frac{\mathrm{d}^2\gamma}{\mathrm{d}s^2} \cos \Theta_e + (F_e^{-1} \cos^2 \Theta_e - 2 \sin \Theta_e) \frac{\mathrm{d}\gamma}{\mathrm{d}s} + \gamma(B - m^2 F_e^{-2} \cos \Theta_e) = \rho^i \Phi^i - \rho^o \Phi^o. \tag{A 16}$$

Writing the normal interface perturbation as

$$\zeta(s) = -\gamma(F_e(s)) \cos \Theta_e(s), \tag{A 17}$$

and substituting into (A 16), we again obtain (16).

Appendix B

The Green function for this problem satisfies the equation:

$$\frac{1}{F_e} \frac{\mathrm{d}}{\mathrm{d}s}\left(F_e \frac{\mathrm{d}G(s\,|\,\xi)}{\mathrm{d}s}\right) + G(s\,|\,\xi)\, q(s, m) = \delta(s - \xi), \tag{B 1},$$

$\delta(s-\xi)$ being the Dirac function. From classical functional analysis, the Green function may be expanded in series of suitably chosen orthogonal functions (Butkov 1968). Thus, using the defined $\zeta_q^*(s)$ space we get

$$G(s\,|\,\xi) = \sum_{q=1}^{\infty} \gamma_q(\xi)\, \zeta_q^*(s), \tag{B 2}$$

where
$$\gamma_q(\xi) = \frac{\zeta_q^*(\xi) F_e(\xi)}{l_q \int_0^{s_0} \zeta_q^*(s)^2 F_e(s)\, ds}, \tag{B 3}$$

by introducing expression (B 2) and the expansion of the Dirac function given by

$$\delta(s-\xi) = \sum_{q=1}^{\infty} \frac{\zeta_q^*(\xi) F_e(\xi)}{\int_0^{s_0} \zeta_q^{*2}(s') F_e(s')\, ds'} \zeta_q^*(s) \tag{B 4}$$

into (B 1). The solution (16)–(19) may thus be expressed using the Green function as follows:

$$\begin{aligned}\zeta(s) &= \int_0^{s_0} G(s\,|\,\xi)\,(\rho^o \Phi^o(\xi) - \rho^i \Phi^i(\xi))\, F_e(\xi)\, d\xi \\ &= \sum_{q=1}^{\infty} \frac{\int_0^{s_0} (\rho^o \Phi^o(\xi) - \rho^i \Phi^i(\xi))\, \zeta_q^*(\xi) F_e(\xi)\, d\xi}{l_q \int_0^{s_0} \zeta_q^{*2}(\xi) F_e(\xi)\, d\xi} \zeta_q^*(s).\end{aligned} \tag{B 5}$$

Appendix C

We use different expansions depending on the meniscus geometry:

(*a*) Bridges (elliptic regime: $\lambda^2 < 1$):

$$\Phi(r,z)^j = A_0^j (r^m + \alpha_0^j r^{-m}) + \sum_{k=1}^{\infty} A_k^j (\alpha_k^j K_m(\beta_k r) + I_m(\beta_k r)) \cos(\mu_k z), \tag{C 1}$$

where I_m and K_m are the modified Bessel functions of the first and second kind, $\mu_k = k\pi/H_0$ (from conditions $w(r, 0) = 0$, $w(r, H_0) = 0$), and α_k^j are for the inner fluid:

$$\alpha_k^i = 0, \quad k = 0, 1, 2, \ldots \tag{C 2}$$

because $u^i(0, z) \neq \infty$; and for the outer fluid:

$$\left.\begin{aligned}\alpha_0^o &= 0, \qquad\qquad m = 0, \\ \alpha_0^o &= R_2^{2m} \frac{1-\lambda}{1+\lambda}, \; m \neq 0,\end{aligned}\right\} \tag{C 3}$$

$$\alpha_k^o = \frac{\beta_k I_{m+1}(\beta_k R_2) + \dfrac{m(1+\lambda)}{R_2} I_m(\beta_k R_2)}{\beta_k K_{m+1}(\beta_k R_2) - \dfrac{m(1-\lambda)}{R^2} K_m(\beta_k R_2)}, \quad k = 1, 2, \ldots \tag{C 4}$$

because $u^o(R_2, z) = 0$.

(*b*) Bridges (hyperbolic regime: $\lambda^2 > 1$):

$$\Phi(r,z)^j = A_0^j (r^m + \alpha_0^j r^{-m}) + \sum_{k=1}^{\infty} A_k^j (\alpha_k^j Y_m(\beta_k r) + J_m(\beta_k r)) \cos(\mu_k z), \tag{C 5}$$

where J_m and Y_m are the Bessel functions of the first and second kind, and α_k^j are for the inner fluid:

$$\alpha_k^i = 0, \quad k = 0, 1, \ldots \tag{C 6}$$

because $u^{i}(0,z) \neq \infty$: and for the outer fluid:

$$\left.\begin{aligned} \alpha_0^{o} &= 0, & m &= 0, \\ \alpha_0^{o} &= R_2^{2m}\frac{1-\lambda}{1+\lambda}, & m &\neq 0, \end{aligned}\right\} \tag{C 7}$$

$$\alpha_k^{o} = \frac{\beta_k J_{m+1}(\beta_k R_2) - \dfrac{m(1+\lambda)}{R_2} J_m(\beta_k R_2)}{\beta_k Y_{m+1}(\beta_k R_2) - \dfrac{m(1-\lambda)}{R_2} Y_m(\beta_k R_2)}, \tag{C 8}$$

because $u^{o}(R_2, z) = 0$.

(*c*) Drops (elliptic regime: $\lambda^2 < 1$):

$$\Phi(r,z)^{j} = A_0^{j} + \sum_{k=1}^{\infty} A_k^{j} J_m(\beta_k r)(\mathrm{e}^{-\mu_k z} + \alpha_k^{j}\,\mathrm{e}^{\mu_k z}), \tag{C 9}$$

where $A_0^{j} = 0$ if $m \neq 0$; β_k is calculated from

$$-\beta_k J_{m+1}(\beta_k r) + \frac{m(1-\lambda)}{r} J_m(\beta_k r)|_{r=R_0} = 0, \tag{C 10}$$

and α_k^{j} is

$$\alpha_k^{i} = \mathrm{e}^{-\mu_k 2(H_0+H_1)}, \tag{C 11}$$

$$\alpha_k^{o} = \mathrm{e}^{\mu_k 2(H_2)}. \tag{C 12}$$

(*d*) Drops (hyperbolic regime: $\lambda^2 > 1$):

$$\Phi(r,z)^{j} = A_0^{j} + \sum_{k=1}^{\infty} A_k^{j} J_m(\beta_k r)\cos(\mu_k(z - H^{j})) \tag{C 13}$$

(*e*) Non-surrounded drops: note that in the above expansions

$$F_e(s) < R_0$$

is assumed for $s \in (0, s_0)$ (see figure 2). These expressions may not be appropriate for geometrical drop configurations where $F_e(z) > 1$ (see figure 1(*c*). In these cases, for non-surrounded drops, it is convenient to take the following expansions:

$$\Phi(r,z) = A_0 r^m + \sum_{k=1}^{\infty} A_k I_m(\beta_k r)(A\cos\mu_k z + B\sin\mu_k z) \tag{C 14}$$

for the elliptic regime, and

$$\Phi(r,z) = A_0 r^m + \sum_{k=1}^{\infty} A_k I_m(\beta_k r)(A\cos\mu_k z + B\sin\mu_k z) \tag{C 15}$$

for the hyperbolic one, where

$$\left.\begin{aligned} A = 1, \quad B = 0, \quad \beta_k &= \frac{k\pi R_0}{2H_0} && k \text{ odd}, \\ A = 0, \quad B = 1, \quad \beta_k &= \frac{(k+1)\pi R_0}{2H_0} && k \text{ even}. \end{aligned}\right\} \tag{C 16}$$

In the case of drops surrounded by an outer medium, and $F_e(z) > 1$ at some point of the interface, we found that it is convenient to expand the velocity and pressure fields in terms of spherical harmonics (Strani & Sabetta 1984).

It is worth mentioning that the use of separation of variables leads to analytical functions which reach very large values within the domains – exponential and modified Bessel functions in the case of the elliptic regime. That represents a difficulty compared to the numerical computation of the series since these functions should be evaluated at the interface, which in general does not lie on a coordinate surface. Despite this, the method has adequate convergence in the range of interest of our analysis. In the elliptic regime, for liquid bridges, the convergence of the method proves to be faster for $\omega \neq 0$ (see (33) and (34)). To understand this, we may consider a new coordinate

$$r^* = r(|1-\lambda^2|)^{\frac{1}{2}},$$

where $\lambda < 1$. Obviously the exponential functions in r decrease, and the convergence is improved.

Nevertheless, the convergence is slower when the coordinate appearing in the exponential-type function is z (see (42) and (46)); a new coordinate

$$z^* = \frac{z}{(|1-\lambda^2|)^{\frac{1}{2}}}$$

may be considered in this case, representing a 'stretching' of the vertical one. This makes the solution by separation of variables in cylindrical coordinates in the case of drops inside a tube impossible for aspect ratios larger than a critical one, H_0^*, which depends on the Weber number.

REFERENCES

Basaran, O. A. & Scriven, L. E. 1989 Axisymmetric shapes and stability of isolated charged drops. *Phys. Fluids* A **1** (5), 795–798.

Boucher, E. A. & Evans, M. J. B. 1975 Pendant drop profiles and related capillary phenomena. *Proc. R. Soc. Lond.* **346**, 349–374.

Brown, R. A. & Scriven, L. E. 1980*a* The shape and stability of rotating liquid drops. *Proc. R. Soc. Lond.* **371**, 331–357.

Brown, R. A. & Scriven, L. E. 1980*b* The shape and stability of captive rotating drops. *Phil. Trans. R. Soc. Lond.* **259**, 51–79.

Busse, F. H. 1984 Oscillations of a rotating liquid drop. *J. Fluid Mech.* **142**, 1–8.

Butkov, E. 1968 *Mathematical Physics.* Addison-Wesley.

Chifu, E., Stan, I., Finta, Z. & Gavrila, E. 1983 Marangoni-type surface flow on an underformable free drop. *J. Colloid Interface Sci.* **93**, 140–150.

Gañán, A. & Barrero, A. 1986 Equilibrium shapes and free vibrations of liquid captive drops. In *Physicochemical Hydrodynamics* (ed. M. G. Velarde), pp. 53–69. Plenum.

Gañán, A. & Barrero, A. 1990 Free oscillations of liquid captive drops. *Microgravity Sci. Technol.* **III** (2), 70–86.

Greenspan, H. P. 1968 *The Theory of Rotating Fluids.* Cambridge University Press.

González, H., McCluskey, F. M. J., Castellanos, A. & Barrero, A. 1989 Stabilization of dielectric liquid bridges by electric fields in the absence of gravity. *J. Fluid Mech.* **206**, 545–561.

Lamb, H. 1932 *Hydrodynamics.* Cambridge University Press.

Miller, C. A. & Scriven, L. E. 1968 The oscillations of a fluid droplet immersed in another fluid. *J. Fluid Mech.* **32**, 417–435.

Myshkis, A. D., Babskii, V. G., Kopachevskii, N. D., Slobozhanin, L. A. & Tyuptsov, A. D. 1987 *Low-Gravity-Fluid Mechanics.* Springer.

Padday, J. F. 1971 The profiles of axially symmetric menisci. *Phil. Trans. R. Soc. Lond.* A **269**, 265.

Pitts, E. 1974 The stability of pendant liquid drops. Part 2. Axial symmetry. *J. Fluid Mech.* **63**, 487–508.

PITTS, E. 1976 The stability of a drop hanging from a tube. *J. Inst. Maths. Applics.* **17**, 387–397.

PLATEAU, J. 1873 *Statique Expérimentale et Théorique des Liquides Soumis aux Seules Forces Moléculaires*. Gauthier-Villars.

RAYLEIGH, LORD 1945 *The Theory of Sound*. Dover.

SANZ, A. 1985 The influence of the outer bath in the dynamics of axisymmetric liquid bridges. *J. Fluid Mech.* **156**, 101–140.

SANZ, A. & LÓPEZ DÍEZ, J. 1989 Non-axisymmetric oscillations of liquid bridges. *J. Fluid Mech.* **205**, 503–521.

STRANI, M. & SABETTA, F. 1984 Free vibrations of a drop in partial contact with a solid support. *J. Fluid Mech.* **141**, 233–247.

STRANI, M. & SABETTA, F. 1988 Viscous oscillations of a supported drop in an immiscible fluid. *J. Fluid Mech.* **189**, 397–421.

VEGA, J. M. & PERALES, J. M. 1983 Almost cylindrical isorotating liquid bridges for small bond numbers. *Proc. 4th European Symp. on Materials Sciences under Microgravity, Madrid, 1983*. ESA SP-191. pp. 247–252.